

Z' boson mass reach and model discrimination at muon colliders

Kateryna Korshynska^{a,1,2,3} , Maximilian Löschner^{b,1} , Mariia Marinichenko^{c,1,2,4} ,
Krzysztof Mękała^{d,1,5} , Jürgen Reuter^{e,1} 

¹Deutsches Elektronen-Synchrotron DESY, Notkestr. 85, 22607 Hamburg, Germany

²Department of Physics, Taras Shevchenko National University of Kyiv, 64/13, Volodymyrska Street, 01601 Kyiv, Ukraine

³Fundamentale Physik für Metrologie FPM, Physikalisch-Technische Bundesanstalt PTB, Bundesallee 100, 38116 Braunschweig, Germany

⁴Instituut-Lorentz, Leiden University, Niels Bohrweg 2, 2333 CA Leiden, The Netherlands

⁵Faculty of Physics, University of Warsaw, Pasteura 5, 02-093 Warszawa, Poland

Received: date / Accepted: date

Abstract We study the discrimination power of future multi-TeV muon colliders for a large set of models with extended gauge symmetries and additional neutral gauge bosons (“ Z' -models”). Our study is carried out using a χ^2 -analysis of leptonic observables of s-channel scattering in effective Z' -models. We make use of angular and chiral asymmetries induced in such models to find the discovery reach of a given muon collider setup in terms of the Z' mass and to discriminate between the different scenarios. In this context, we discuss how polarized beams – should they become available at muon colliders – or polarization measurements can help in the discrimination. Our results show that typical muon collider setups which are currently under consideration can give a significantly higher reach compared to existing bounds and projections for high-luminosity LHC.

1 Motivation

The Standard Model (SM) of particle physics is among the most well-tested theories to date and can explain experimental observations to unprecedented precision despite thorough searches for deviations at modern collider experiments. Nonetheless, several well-known phenomena such as the nature of dark matter, the baryon-antibaryon asymmetry of the universe or even the universal law of gravity lack an explanation within this theory. To accommodate for effects Beyond the Standard Model (BSM), multiple extensions of the current formulation have been proposed. If such extensions are based on new gauge symmetries, the existence of additional neutral gauge bosons (which we denote as Z') is

the natural consequence. In the absence of a unique well-motivated ultra-violet (UV) complete BSM theory, simplified models or effective theories can be useful tools to study potential deviations from SM predictions in a generic way. An example of this is the effective Z' -model with new gauge boson couplings to the SM fermions, as discussed e.g. in [1–3]. The idea is that an experimental determination of such couplings could eventually give guidance toward a specific UV-complete model which in turn might help explain other observational phenomena.

Recent measurements at the LHC have excluded the existence of a Z' boson with a mass up to about 5 TeV [4–11], which will be raised to close to 8 TeV [12]. Several ways to search for neutral gauge bosons have also been considered for future e^+e^- colliders which, mainly due to a cleaner collision environment, could probe masses up to about 20 TeV, depending on the collider energy [2, 13–22]. Given recent progress in the development of the muon collider accelerator design, the possibility of searching for heavy particles at such a multi-TeV machine is an appealing idea and has already been considered in [23] where several resonance production channels have been studied.

A multi-TeV muon collider has been proposed as the next energy-frontier collider in high-energy physics, combining the clean environment of e^+e^- machines with the energy reach of hadron colliders. Recent technological progress, especially in muon cooling [24], has led to a high priority in the US Snowmass Community Summer Study [25–28] and the Particle Physics Project Prioritization Panel (P5) report [29]. In Europe, the International Muon Collider Collaboration (IMCC) is leading the European effort, suggested in the last European Particle Physics Strategy Update (EPPSU 2020) [30, 31].

A comprehensive, systematic study of the indirect discovery reach of future muon colliders for heavy neutral gauge bosons originating from different unification scenar-

^akateryna.korshynska@desy.de

^bmaximilian.loeschner@desy.de

^cmariia.marinichenko@desy.de

^dkrzysztof.mekala@desy.de

^ejuergen.reuter@desy.de

ios has been missing in the literature. We address the issue in this paper by proposing a framework based on leptonic observables suitable not only for searches for a Z' boson but also for specifying its nature. The work is structured as follows: in Section 2, we review models introducing additional neutral gauge bosons and in Section 3, we explain why future muon colliders may be used to search for them. In Section 4, we present our analysis procedure whose results are discussed in Section 5. The most important findings of the work are summarized in Section 6.

2 Theoretical background

In this section, we present the models considered in our study which contain additional neutral gauge bosons beyond the SM and review the relevant aspects of their phenomenology. Such a collection can of course never be complete, but we give a well-defined selection of different kinds of weakly and strongly-coupled models to cover theory space as comprehensively as possible.

2.1 Gauge bosons beyond the Standard Model

The Standard Model can be formulated as the most general renormalizable quantum field theory invariant under the gauge group $\mathcal{G}_{SM} = SU(3)_c \times SU(2)_L \times U(1)_Y$ with the matter content discovered as of today. The symmetry under this group gives rise to the existence of the well-known gauge bosons: g, W^\pm, Z, γ . Leaving gravity aside, it remains an open question whether \mathcal{G}_{SM} represents the complete symmetry group responsible for what we can observe in Nature. It is possible that it merely represents the broken version of an enlarged symmetry group or *Grand Unified Theory* (GUT) [32–35] which in turn could lead to the existence of additional gauge bosons among other new particles. In general, any extension of the SM involving the introduction of additional gauge symmetries might extend the gauge boson sector [2]. The rich phenomenology of such models, reviewed for example in [3], could be connected to flavor non-universality [36, 37], neutrino masses [38–43] or the dark-matter problem [44–48].

Since no direct hint towards a single specific model with enlarged gauge symmetry has been experimentally found to date, we study a variety of models in a general way, namely in terms of the phenomenology of additional heavy neutral gauge bosons they would ensue. Therefore, we use an effective Z' -model where we introduce a Z' with couplings to the SM fermions that are the only trace of New Physics. In this model, the interactions of the neutral gauge bosons with the SM fermions are given by the generic neutral-current La-

grangian: [2, 3, 22, 49]:

$$\begin{aligned} -\mathcal{L}_{NC} &= eA_\mu J_A^\mu + g_Z Z_\mu J_Z^\mu + g_{Z'} Z'_\mu J_{Z'}^\mu, \\ J_A^\mu &= \sum_f \bar{f} \gamma^\mu q_f f, \\ J_Z^\mu &= \sum_f \bar{f} \gamma^\mu (v_f^{SM} - \gamma_5 a_f^{SM}) f, \\ J_{Z'}^\mu &= \sum_f \bar{f} \gamma^\mu (v_f - \gamma_5 a_f) f, \end{aligned} \quad (1)$$

where f denotes the SM fermions, A is the photon, Z is the SM neutral gauge boson, Z' is the new heavy neutral boson, e is the positron charge, g_Z and $g_{Z'}$ are the gauge couplings of the corresponding bosons, q_f is the fermion electric charge in units of e , v_f^{SM} and a_f^{SM} are the vector and axial-vector coupling of the fermion to the SM neutral boson and v_f and a_f are the couplings to the new neutral boson. Note that the splitting of the couplings into a prefactor $g_{Z'}$ and vector-/axial-vector components v_f, a_f , while customary for the SM, is rather arbitrary for a generic Z' model. Our convention will become clear below.

2.2 The set of Z' -models considered

In our analysis, we consider a vast set of BSM models, including the Sequential Standard Model (denoted as SSM) [50–52], the E6 Model (E6) [53, 54], the Left-Right Symmetric Model (LR) [33, 43, 55, 56], the Alternative Left-Right Model (ALR) [57, 58], the Littlest Higgs Model (LH) [59–61], the Universal Simplest Little Higgs Model (USLH) [62–64], and the $U(1)_X$ Model [65, 66]. While the SSM cannot be embedded into a renormalizable GUT-like model, it has become a standard candle for Z' searches with over-optimistically large couplings; for this reason, we keep it in our selection of models. Many early GUT models that were inspired by an embedding into a low-energy superstring action exhibit E_6 as a GUT gauge group. Several breaking scenarios via intermediate groups like $SU(5)$ [32], $SO(10)$ [67], Pati-Salam $SU(4) \times SU(2) \times SU(2)$ [33], or trification $SU(3)^3$ [68] have been studied, and the rank reduction from six to four for the SM gives rise to two potential Z' candidates. The simplest class of models is left-right (LR)-symmetric models, which appear as low-scale effective theories of Pati-Salam or trification likewise. Multi-step breaking with several GUT scales has been considered [69, 70], and so have the effects of mixing between different Z' bosons, both on model discrimination and reconstruction of the UV-scale model [71, 72]. Besides weakly-coupled, GUT-inspired models, there is the large class of models of compositeness or partial compositeness where some of the additional symmetries in the strongly-coupled sector have been gauged to avoid too light or massless Nambu-Goldstone models. One class of models is Little Higgs models, while another class of strongly-

Model	$g_{Z'}$	$2v_l$	$2a_l$
SSM	$\frac{e}{s_W c_W}$	$2s_W^2 - \frac{1}{2}$	$-\frac{1}{2}$
E_6	$\frac{e}{c_W}$	$\frac{2\cos\beta}{\sqrt{6}}$	$\frac{\cos\beta}{\sqrt{6}} + \frac{\sqrt{10}\sin\beta}{6}$
LR	$\frac{e}{c_W}$	$\frac{1}{\alpha} - \frac{\alpha}{2}$	$\frac{\alpha}{2}$
ALR	$\frac{e}{s_W c_W \sqrt{1-2s_W^2}}$	$\frac{5}{2}s_W^2 - 1$	$-\frac{1}{2}s_W^2$
LH	$\frac{e}{s_W}$	$-\frac{c}{4s}$	$-\frac{c}{4s}$
USLH	$\frac{e}{c_W \sqrt{3-4s_W^2}}$	$\frac{1}{2} - 2s_W^2$	$\frac{1}{2}$
$U(1)_X$	$\frac{e}{4c_W}$	-8	2

Table 1: The Z' couplings to leptons in the models considered in this paper. The sine of the Weinberg angle is denoted by s_W . For the description of the models and the explanation of the model-specific parameters see the main text. The table and notation are adapted from [22].

coupled models via their dual description to warped extra dimensions [73] directly interpolates into models with additional space-time dimensions like e.g. universal extra dimensions [74, 75].

For simplicity, we assume that all the considered models are flavor-universal, *i.e.* the couplings do not differ between the three fermion generations. The scenarios considered are listed in Table 1 where we present the respective axial and vector couplings of the Z' to the fermions together with the absolute normalization of the couplings, $g_{Z'}$. For the E_6 models, the specific values of the mixing angle $\beta = 0, \pi/2, \arctan(-\sqrt{5/3})$ correspond to the so-called χ, ψ and η models. We use $\beta = 0$ in our analysis as a representative case. For the LR model, the mixing angle between the two $SU(2)$ groups has to be in the range $\sqrt{2/3} \leq \alpha \leq \sqrt{c_W^2/s_W^2} - 1$, and we use the upper bound for α . For the LH model, the mixing angles between the two $SU(2)$ groups obey $1/10 \leq c/s \leq 2$, and we use $c/s \equiv 1$.

2.3 Observables

The models under consideration specify different points in the parameter space of axial and vector couplings to fermions. Therefore, we study observables which encode angular and chiral properties in order to distinguish between the different scenarios. The analysis is particularly simple in leptonic scattering channels because all of the models considered are flavor universal so that only two coupling factors enter the scattering amplitudes (as opposed to the production of hadrons where leptonic and hadronic axial and vector couplings would play a role, and couplings of up- and down-type quarks would be overlaid). This makes it possible to study the models in the two-dimensional a_l - v_l plane with the only other unknown being the mass of the Z' (in prin-

ciple, another additional parameter would be the Z' width, but we will only consider Z' states heavier than the collider energy such that the width does not have a significant impact on any observable). The experimental observables we consider are:

1. the total cross-section for the process $\mu^+\mu^- \rightarrow f\bar{f}$, denoted as σ^f , for $f \in \{e, \tau\}$ (we do not consider μ final states due to the contamination from t -channel exchange);
2. the forward-backward asymmetry, defined as:

$$A_{FB}^f = \frac{\sigma_F^f - \sigma_B^f}{\sigma^f}, \quad (2)$$

where, for $f \in \{e, \tau\}$:

- σ_F^f – the partial cross section for the fermion f going in the forward direction,

$$\sigma_F^f = \int_0^1 d\cos\theta \frac{d\sigma}{d\cos\theta}(\mu^-\mu^+ \rightarrow f\bar{f}) \quad (3)$$

- σ_B^f – the partial cross section for the fermion f going in the backward direction;

$$\sigma_B^f = \int_{-1}^0 d\cos\theta \frac{d\sigma}{d\cos\theta}(\mu^-\mu^+ \rightarrow f\bar{f}) \quad (4)$$

3. the left-right asymmetry, defined as:

$$A_{LR}^f = \frac{\sigma_{LR}^f - \sigma_{RL}^f}{\sigma^f}, \quad (5)$$

where, for $f \in \{e, \tau\}$:

- $\sigma_{LR}^f = \sigma(\mu_L^-\mu_R^+ \rightarrow f\bar{f})$ – the partial cross section for the fully left-polarized muon beam and right-polarized antimuon beam,
- $\sigma_{RL}^f = \sigma(\mu_R^-\mu_L^+ \rightarrow f\bar{f})$ – the partial cross section for the fully right-polarized muon beam and left-polarized antimuon beam;

We will comment on the possibility of polarization at the muon collider below.

4. the polarization asymmetry, defined as:

$$A_{pol}^f = \frac{\sigma_{lh}^f - \sigma_{rh}^f}{\sigma^f}, \quad (6)$$

where, for $f = \tau$:

- $\sigma_{lh}^f = \sigma(\mu^-\mu^+ \rightarrow \tau_L^-\tau_R^+)$ – the partial cross section for the left-handed fermions in the final state,
- $\sigma_{rh}^f = \sigma(\mu^-\mu^+ \rightarrow \tau_R^-\tau_L^+)$ – the partial cross section for the right-handed fermions in the final state.

Note that for massless fermions, $A_{pol}^f = A_{LR}^f$ holds [2] but we keep them as two independent quantities due to their vastly different experimental measurement. This will manifest itself in our statistical analysis via different systematic uncertainties.

In accelerator physics, it is not possible to fully polarize lepton beams and Eq. (5) should be corrected by a factor of the effective polarization

$$P_{\text{eff}} = \frac{P^+ + P^-}{P^+ P^- + 1}, \quad (7)$$

where P^- (P^+) is the polarization fraction for the (anti-) muon beam and we assume opposite polarizations for the two beams. Analogously, fully perfect flavor tagging and τ polarization measurements are not possible and their efficiencies contribute to the systematic uncertainty of the study. Since the Muon Collider project is still in a preliminary phase, we tackle the issue by postulating an overall systematic uncertainty to 1% which roughly matches the order of magnitude of the statistical uncertainty. The polarization asymmetry is an exception though, because its uncertainty within the LEP measurements is much larger than other systematic uncertainty [76, 77]. Therefore, we conservatively assume a systematic uncertainty of 5% here. The impact of assuming different values is briefly discussed in Appendix A.

In the current scope of the analysis, we ignore additional information from studying hadronic observables. Their usage provides valuable input for the model discrimination; however, in view of the leptonic production channel at the muon collider, disentangling different products of couplings entering the expressions of our observables, including tagging and separating light up- and down-quark flavors, requires additional assumptions in our statistical analysis. This is beyond the scope of the present study. There is recent progress in tagging light-quark flavors using final-state QED radiation (see e.g. [78]), which would enable to partially disentangle these light-quark flavor couplings. We will extend the study towards hadronic observables in the future.

3 High-energy muon collider setup

For a sustainable future in high-energy collider physics, long-term planning is unavoidable. The high-luminosity upgrade of the Large Hadron Collider (HL-LHC) is now approved [79] which, after a decade of running, could run temporarily with the start-up phase of or will be followed by an e^+e^- Higgs factory [29, 31, 80–85]. On a 20-year time scale, ambitious projects for parton collisions at energies of ~ 10 TeV could be realized either with a 100-TeV hadron machine [86–88] or a multi-TeV muon collider [30]. Since the latter has recently regained attention due to the successful demonstration of the muon-cooling principles [89], we decided to consider this proposal in our study, as already alluded to in the introduction.

Muon colliders would offer a versatile environment for both precision studies of SM and BSM phenomenology and

high-energy searches, including the possible occurrence of new physics in electroweak interactions. Muons can be efficiently accelerated in circular machines, as they are more than 200 times more massive than electrons which significantly reduces bremsstrahlung. On the other hand, contrary to protons, muons are elementary, point-like particles offering a much cleaner collision environment¹. Nevertheless, their finite lifetime poses a challenge for the design of both the accelerator complex and the detector. For brevity, we will simplify the discussion of the experimental effects in the following, assuming global systematic uncertainties only and leaving the meticulous study of the experimental conditions to the time when the final detector designs are available.

The muon collider community currently aims at achieving a collision energy of 10 TeV with a future machine [30]. An initial stage of 3 TeV is foreseen on the path towards the targeted energy and possible extensions of the project are not excluded if technology permits. As for the current design of the accelerator complex, the integrated luminosity, \mathcal{L}_{int} , scales with the square of the collision energy, E_{CM} . The results presented below scale mostly trivially with the integrated luminosity, and different running scenarios can be easily deduced. In our analysis, we assume that a 10-TeV muon collider would deliver 10 ab^{-1} of data which can be extrapolated to other energies by taking:

$$\mathcal{L}_{\text{int}}(E_{\text{CM}}) = 10 \text{ ab}^{-1} \left(\frac{E_{\text{CM}}}{10 \text{ TeV}} \right)^2. \quad (8)$$

The default setup of the muon collider does not assume polarization of the muon beams. However, due to the production of muons from pion decays there is a certain level of polarization inherent in the beams, and circular lepton colliders automatically build up transverse polarization. This could be converted into longitudinal polarization using spin rotators which has been discussed in the technical accelerator reports. Therefore, we will also consider the possibility of 30% polarization of both beams.

4 Analysis procedure

In this section, we present our analysis procedure. We demonstrate a statistical framework that we use to set limits on the Z' masses which could be probed at a future muon collider and show how one can distinguish between different models of New Physics. We carry out the analysis in the Born approximation which was shown to give reliable results in off-peak regions of the relevant observables, as long as appropriate kinematic cuts on photon radiation are applied [2].

¹Note, however, the electroweak partonic content inside muons when applying a collinear factorization picture to high-energy collisions [90–92]

4.1 Mass reach

Our statistical analysis is based on the χ^2 -test statistic:

$$\chi^2(a, v, M_{Z'}) = \sum_{i=1}^{n_{ob}} \left[\frac{O_i^{\text{SM}} - O_i(a, v, M_{Z'})}{\Delta O_i^{\text{SM}}} \right]^2 + n_{ob}, \quad (9)$$

where n_{ob} is the number of observables used, O_i^{SM} is the value of the i -th observable predicted by the SM, $O_i(a, v, M_{Z'})$ is the value of the observable in a given model (defined uniquely by a pair of axial and vector couplings, (a, v) , and the Z' mass, $M_{Z'}$)² and ΔO_i^{SM} is the measurement uncertainty, $\Delta O_i^{\text{SM}} = \sqrt{\Delta O_{i,\text{stat}}^2 + \Delta O_{i,\text{sys}}^2}$ for $\Delta O_{i,\text{stat}}$ and $\Delta O_{i,\text{sys}}$ being the statistical and systematic uncertainties, respectively. The term “ $+n_{ob}$ ” in Eq. (9) comes about via fluctuations of experimental values around the theory expectations of the O_i^{SM} . We show in Appendix B that this simple approach perfectly coincides with the procedure of performing hundreds of pseudo-experiments to mimic real measurements by extracting observables from normal distributions. That this is indeed a meaningful framework can also be seen by assuming that a given model shows no significant discrepancy from the SM (*i.e.* the difference between all the observables is zero by construction) which also means the first term gives no contribution to the total value and the true expected value of the χ^2 distribution can only be restored by the second term.

In the following, we will assume that the statistical uncertainties are given by [14]:

$$\Delta \sigma^f = \frac{\sigma^f}{\sqrt{N_f}}, \quad (10a)$$

$$\Delta A_{FB}^f = \sqrt{\frac{1 - (A_{FB}^f)^2}{N_f}}, \quad (10b)$$

$$\Delta A_{LR}^f = \sqrt{\frac{1 - (P_{\text{eff}} A_{LR}^f)^2}{N_f P_{\text{eff}}^2}}, \quad (10c)$$

$$\Delta A_{pol}^f = \sqrt{\frac{1 - (A_{pol}^f)^2}{N_f}}, \quad (10d)$$

where P_{eff} is the polarization fraction of the initial state lepton, as defined in Eq. (7), and $N_f = \mathcal{L}_{\text{int}} \cdot \sigma^f$ is the number of expected events.

Given the design status of a future muon collider, a complete assessment of the systematic uncertainties is currently not possible. Therefore, for sake of simplicity of the analysis, we will assume that the measurement is statistically limited and the corresponding systematic uncertainties do not

²For brevity, we will drop the parameters whenever there is no danger of confusion.

exceed significantly the statistical error. Thus, our analysis may be perceived as a hint of what the desired detector performance should be. In Appendix A, we show the impact of varying the systematic errors.

We assume that a model gives predictions distinct from the SM if the value of the χ^2 test exceeds the critical value at the confidence level of 95% for the given number of degrees of freedom, $n_{\text{d.o.f.}}$, $\chi^2(a, v, M_{Z'}) > \chi_{\text{crit}}^2(n_{\text{d.o.f.}})$. In our analysis, we combine seven observables, namely:

- 1-2. the total cross section, σ^f , for $f \in \{e, \tau\}$,
- 3-4. the forward-backward asymmetry, A_{FB}^f , for $f \in \{e, \tau\}$,
- 5-6. the left-right asymmetry, A_{LR}^f , for $f \in \{e, \tau\}$,
7. the polarization asymmetry, A_{pol}^f , for $f = \tau$,

as defined in Sec. 2.3. For the mass reach, we have $\chi_{\text{crit}}^2(n_{\text{d.o.f.}} = 7) = 12.02$ which corresponds to the 90%-quantile because it is a one-sided test, while for the resolution power discussed in the next section, we have $\chi_{\text{crit}}^2(n_{\text{d.o.f.}} = 7) = 14.07$.

4.2 Resolution power

The resolution power measures the compatibility of a fictitious measurement of a parameter pair (a, v) for a fixed $M_{Z'}$ with a given reference Z' -model with couplings $(a_{\text{model}}, v_{\text{model}})$. Should the measurement of the couplings fall outside the region where $\chi_{\text{model}}^2 < \chi_{\text{crit}}^2(n_{\text{d.o.f.}})$, we can distinguish it from the theoretical prediction and thus, exclude the given model at the 95% confidence level. As in this case, our measurement is compared to a particular model, the test statistic given in Eq. (9) should be replaced by:

$$\chi_{\text{model}}^2(a, v, M_{Z'}) = \sum_{i=1}^{n_{ob}} \left[\frac{O_i^{\text{model}} - O_i(a, v, M_{Z'})}{\Delta O_i^{\text{model}}} \right]^2 + n_{ob}, \quad (11)$$

where the only difference comes from the fact that the SM value of an observable is replaced by the observable predicted within the given model, O_i^{model} .

5 Results

The results presented in the following two subsections are obtained by determining values for each observable analytically using the full $(\mu^+ \mu^- \rightarrow \ell^+ \ell^-)$ -scattering amplitudes for $\ell \in \{e, \tau\}$ in Born approximation shown in Figure 1. We also include the width of the Z' using the Born approximations defined in [2]. The values for $\Gamma(Z' \rightarrow \text{any})$ range from ~ 40 GeV (USLH) to ~ 300 GeV (SSM) for $M_{Z'} = 30$ TeV. The exact width of the Z' does not play a major role in the analysis though, because the bounds we find are driven by the off-peak regions of the observables.

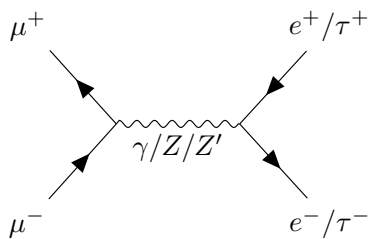


Fig. 1: The set of Feynman diagrams entering our χ^2 -analysis.

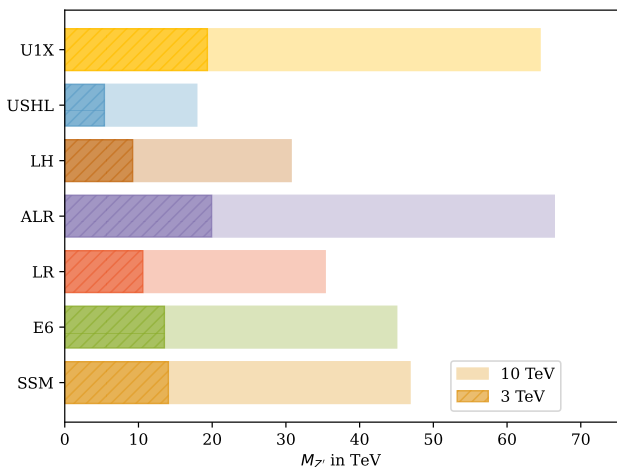


Fig. 2: The reach in $M_{Z'}$ for a 3 TeV and 10 TeV muon collider with luminosities of 0.9 ab^{-1} and 10 ab^{-1} , respectively for $P_{\text{eff}} = 0$, $\Delta_{i,\text{sys}} = 1\%$ for σ_f, A_{FB}, A_{LR} and $\Delta_{A_{\text{pol}},\text{sys}} = 5\%$. The bars correspond to the exclusion limit of the given Z' -model at 95% confidence level.

We use Eq. (8) to set the integrated luminosity. Then, the statistical errors of Eq. (10) are typically of $\mathcal{O}(1\%)$ or lower (for $M_{Z'} = 3\sqrt{s}$). This could serve as a target value for the systematic errors of the prospective collider measurements in order for the precision to be driven by statistical fluctuations rather than systematics.

Cross-checks of the results obtained in this way were carried out in the Monte Carlo event generator framework Whizard 3.1 [93, 94], using the included generic Z' -model implementation as well as its UFO interface [95–97]. Note that the latter can in principle be used for more sophisticated event-level analyses, potentially also beyond the Born approximation [98], or involving detector simulation, but at the cost of higher computational effort. This is beyond the scope of this current study.

5.1 Mass reach

In Figure 2, we show the mass reach we find using the analysis procedure explained in Sec. 4. It shows that using leptonic observables alone, the exclusion limits at 95% C.L. for a 10 TeV muon collider extend up to $\sim 70 \text{ TeV}$, depending on the model. We find relatively low exclusion limits of $\sim 17 \text{ TeV}$ for the Little/Littlest Higgs models due to the small magnitude of the leptonic axial and vector couplings³. The results shown are without beam polarization as the default setup of the muon collider, and because we find that even for polarization fractions close to 100%, the limits do not change significantly, *i.e.* only by up to 3%. This is due to the limited statistical significance of A_{LR} , *i.e.* a higher statistical error compared to A_{FB} (see Eq. (10)). The influence of the polarization fraction becomes important for the model discrimination though, as explained in the following section.

The discussion of [14] for e^+e^- colliders shows that the inclusion of hadronic observables can increase the reach by up to $\sim 50\%$, depending on the model. An example is the SSM, where one has axial and vector couplings to up- and down-type quarks of relatively large magnitude. The effect is much less drastic for models with smaller quark couplings though, such as the $U(1)_X$. For muon colliders, we expect a similar increase in mass reach when including hadronic observables.

5.2 Resolution power

Here, we determine the resolution power of a 10 TeV muon collider in the off-peak region of the observables considered, *i.e.* for masses above the collider energy. A study in the peak region would require a different type of analysis and for even smaller masses, a study for precision e^+e^- machine would be more sensible. In Figure 3, we show the resolution power for Z' -axial and -vector couplings, given that a signal for a Z' has been found at a mass $M_{Z'}$ of either 40 TeV, 30 TeV or 15 TeV. We find that one would be able to discriminate to a good extent between the models considered at around $M_{Z'} \sim 30 \text{ TeV} = 3\sqrt{s}$ or lower. Already for masses slightly higher than that, the discrimination power starts to decrease rather rapidly. On the other hand, it grows very fast for lower masses because the closer the Z' -mass is to the collider energy, the more one approaches the Z' -pole where deviations from the SM become substantial. Then, models with axial or vector couplings of comparatively large magnitude can be discriminated even without the use of polarized beams or a very accurate measurement of the τ polarization. In Appendix A, we discuss the influence of the latter measurements in more detail.

³Note that in such a case also the current LHC bounds are weaker as the signal strengths in Drell-Yan searches is reduced.

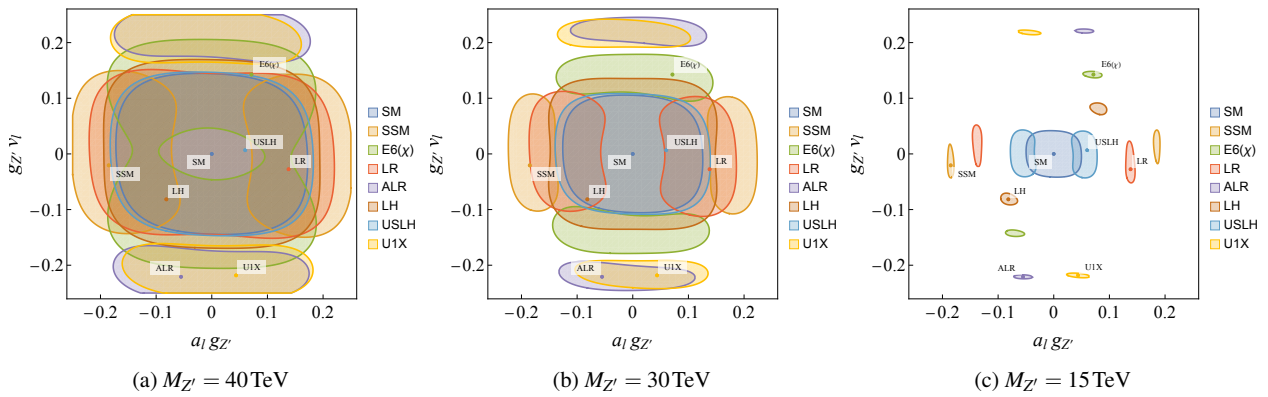


Fig. 3: Resolution power for different masses of the Z' . Inputs: $\mathcal{L}_{\text{int}} = 10\text{ab}^{-1}$, $E_{\text{CM}} = 10\text{TeV}$, $P_{\text{eff}} = 0$.

6 Conclusions

A Z' boson occurs in a variety of BSM theories that are based on extensions of the SM gauge group. We showed that at a muon collider, using indirect search methods for leptonic observables alone, one would be able to probe Z' masses of up to $\sim 70\text{TeV}$. For masses up to $\sim 30\text{TeV}$, the same framework can be applied to discriminate its nature in terms of its axial and vector couplings to fermions, pointing towards a specific model of New Physics. The presented results give the most stringent limits up to date. Employing hadronic observables has been left for future explorations. They are expected to enhance the discovery reach towards higher Z' masses but are not expected to improve the model discrimination by a lot, as they suffer from combinatorics between light up- and down-type quarks. Final states consisting of charm and bottom will add discrimination power but are more complicated to quantify due to the charm- and bottom-tagging efficiencies. Z' decays into top quarks are highly interesting, especially for models where the top coupling is special (e.g. the Littlest Higgs or top-color models), but clearly these final states go beyond the simple two-fermion signatures considered here. Note that another complication is the non-factorization of leptonic production current and hadronic decay current.

A spectacular level of model discrimination is already possible using the default setup of the muon collider, using left-right and τ polarization asymmetries. If the systematic error on the τ polarization measurement dominates over its statistical uncertainty significantly, beam polarization of a degree of up to 30% via spin rotators could enhance the discriminative power as it allows to use left-right asymmetries as well.

As statistical uncertainties can be expected to be of the order of 1%, we show that it is crucial to have the systematic uncertainties under control in order to guarantee a good model discrimination. This means that systematic uncertainties from lepton charge determination, angular resolution, τ

polarization measurements etc. should not exceed a percent by much. This provides a ballpark what future muon collider detector development should aim for.

Acknowledgments

The work of KM and JRR was partially supported by the National Science Centre (Poland) under the OPUS research project no. 2021/43/B/ST2/01778. ML, KM and JRR acknowledge the support of the Deutsche Forschungsgemeinschaft (DFG, German Research Association) under Germany's Excellence Strategy-EXC 2121 "Quantum Universe"-390833306. KK and MM acknowledge Deutsches Elektronen-Synchrotron (DESY) for a hospitable environment during the DESY Ukraine Winter School. This work has also been funded by the Deutsche Forschungsgemeinschaft (DFG, German Research Foundation) – 491245950. Furthermore, we acknowledge support from the COMETA COST Action CA22130.

Appendix A: Parametric variations of resolution power

In this Appendix, we present a list of plots for the discrimination power in the $a_l \cdot v_l$ plane of Z' models for variations of different input values. In Figure 4, we show that adding a polarization measurement or polarized beams to the analysis enables the distinction of models with different relative signs between the axial and vector couplings, e.g. between the ALR and $U(1)_X$ models. A simultaneous sign change of the axial and vector couplings would remain undetectable, because the left-right asymmetry A_{LR} only adds sensitivity to the product $a_l \cdot v_l$ [2]. Comparing Figure 4b to Figure 4c, we see that one can achieve similar resolutions by either bringing the systematic uncertainty on the τ polarization down to the 1%-level or by using polarized muon beams with $P_{\text{eff}} = 30\%$. Moreover, we find that a further increase

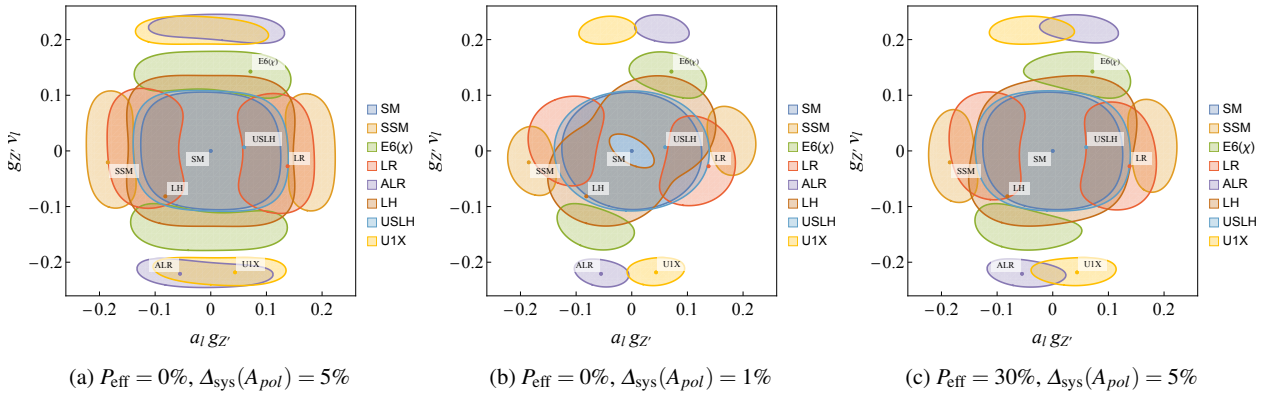


Fig. 4: Resolution power for different combinations of effective polarizations and systematic errors for the τ polarization asymmetry. Inputs: $\mathcal{L}_{\text{int}} = 10 \text{ ab}^{-1}$, $E_{\text{CM}} = 10 \text{ TeV}$, $M_{Z'}$ = 30 TeV.

in the effective polarization does not yield a significant increase in the resolution power. In [Appendix C](#), we show how the individual observables contribute to the resolution power and present their analytic form in [Appendix D](#).

In [Figure 5](#) we show the variations for three different values of the systematic errors. We find that at $\sim 1\%$, systematic errors become competitive both with the statistical ones by explicit comparisons of the errors magnitudes, as well as by noticing that even a strong reduction in the systematic error does not increase the discrimination power significantly, as then the measurement becomes limited by statistics.

We do not show the variation of other parameters explicitly here, because their influence can be inferred from the variations of the parameters discussed. The variation of the collider energy yields similar changes as shown in [Figure 3](#), namely that the closer the energy is to the mass of the Z' , the better the discrimination power will be. A variation of the luminosity solely affects the magnitude of the statistical errors. Therefore, a decrease in luminosity will lead to larger errors and similar behavior as shown in [Figure 5](#).

Appendix B: Test statistics derivation

In this section, we discuss the origin of the shift in our χ^2 -distributions by the number of observables, as it appears in [Eq. \(9\)](#) and [Eq. \(11\)](#). Let us call the pseudo-measurement of an observable for a given reference model \hat{O}_i and the corresponding theory prediction O_i with the error ΔO_i and assume that they follow the normal distribution

$$f(\hat{O}_i) = \exp\left[-\frac{(\hat{O}_i - O_i)^2}{\Delta O_i^2}\right] \frac{1}{\Delta O_i \sqrt{2\pi}}. \quad (\text{B.1})$$

This means that the expectation value for \hat{O}_i is

$$\langle \hat{O}_i \rangle = O_i \quad (\text{B.2})$$

and the variance

$$\langle (\hat{O}_i - O_i)^2 \rangle = \Delta O_i^2. \quad (\text{B.3})$$

We can also expand the variance:

$$\langle (\hat{O}_i - O_i)^2 \rangle = \langle \hat{O}_i^2 \rangle - 2\langle \hat{O}_i \rangle O_i + O_i^2 = \langle \hat{O}_i^2 \rangle - O_i^2, \quad (\text{B.4})$$

and therefore rewrite:

$$\langle \hat{O}_i^2 \rangle = O_i^2 + \Delta O_i^2. \quad (\text{B.5})$$

If we now determine the expectation value for χ^2 to test a model with observables O_i^{test} and insert [Eq. \(B.5\)](#), we find

$$\langle \chi^2 \rangle = \sum_{i=1}^{n_{ob}} \left\langle \frac{(\hat{O}_i - O_i^{\text{test}})^2}{\Delta O_i^2} \right\rangle = \sum_{i=1}^{n_{ob}} \frac{(O_i - O_i^{\text{test}})^2}{\Delta O_i^2} + n_{ob}, \quad (\text{B.6})$$

where the shift by n_{ob} appears due to the second term in [Eq. \(B.5\)](#) and explains why it is included in [Eq. \(9\)](#) and [Eq. \(11\)](#). This is equivalent to the outcome when averaging over a large number of pseudo-measurements when drawing values from [Eq. \(B.1\)](#) randomly using a Monte Carlo algorithm.

Appendix C: Resolution power of individual observables

In [Figure 6](#), we show the resolution power of the individual observables σ_{tot} , A_{FB} and A_{LR} . The total cross section gives elliptic resolution regions while the two asymmetries give distinct hyperbolic regions. This can be understood by the dependence of the observables on either the sum of the squares of axial and vector couplings (σ_{tot}), the difference of the squares (A_{FB}) or their product (A_{LR}) in the Born approximation [\[14\]](#). In comparison to the approximate bounds for the observables used in [\[14\]](#), we see slight asymmetries in the bounding regions as a result of using the full Born amplitudes. They are nevertheless in very good agreement with the approximate bounds.

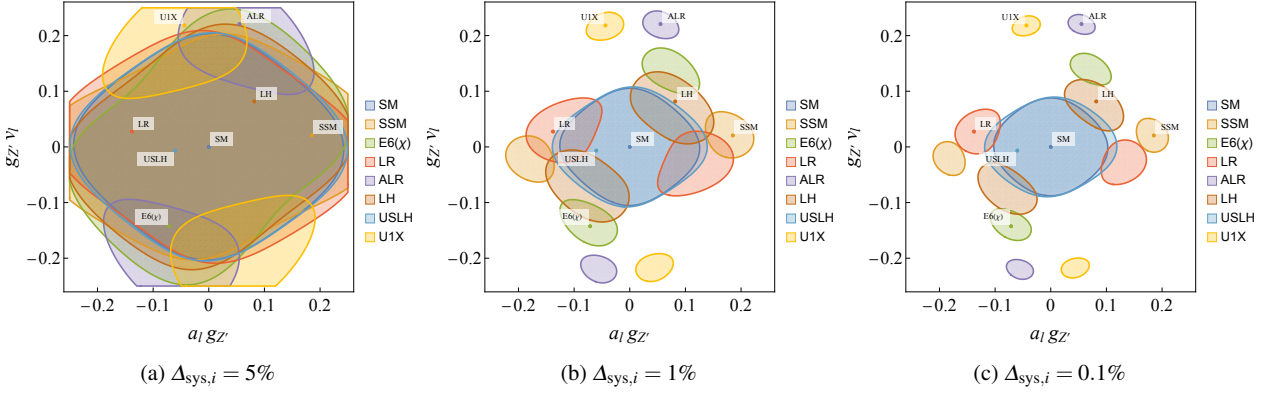


Fig. 5: Resolution power for different systematic errors. Inputs: $\mathcal{L}_{\text{int}} = 10 \text{ ab}^{-1}$, $E_{\text{CM}} = 10 \text{ TeV}$, $M_{Z'} = 30 \text{ TeV}$, $P_{\text{eff}} = 80\%$.

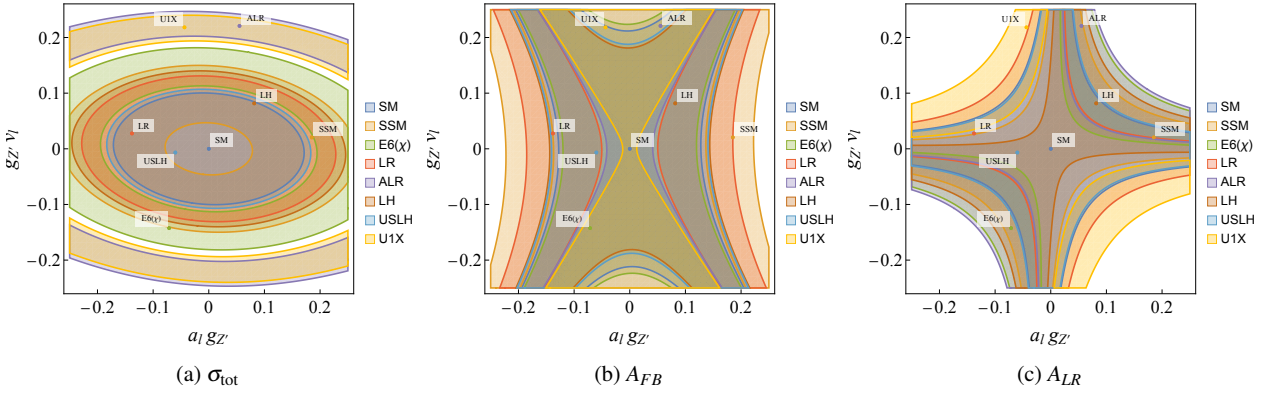


Fig. 6: Resolution power of individual observables. Inputs: $\mathcal{L}_{\text{int}} = 10 \text{ ab}^{-1}$, $E_{\text{CM}} = 10 \text{ TeV}$, $M_{Z'} = 30 \text{ TeV}$.

Appendix D: Asymmetries

Here we present expressions for left-right and forward-backward asymmetries in terms of individ-

ual interference diagrams (see Fig. 1) for a high-energy machine (*i.e.* we neglect the masses of the fermions). The forward-backward asymmetry reads

$$A_{FB}^f(s) = \frac{1}{8\pi s \sigma^f(s)} \left\{ 2g_Z^4 a_\mu^{SM} a_f^{SM} v_\mu^{SM} v_f^{SM} |\chi_Z|^2 + 2g_Z^4 a_\mu a_f v_\mu v_f |\chi_{Z'}|^2 + q_\mu q_f e^2 \left(g_Z^2 a_\mu^{SM} a_f^{SM} \text{Re}(\chi_\gamma \chi_{Z'}^*) + g_{Z'}^2 a_\mu a_f \text{Re}(\chi_\gamma \chi_{Z'}^*) \right) + g_Z^2 g_{Z'}^2 (a_\mu^{SM} v_\mu + a_\mu v_\mu^{SM}) (a_f^{SM} v_f + a_f v_f^{SM}) \text{Re}(\chi_Z \chi_{Z'}^*) \right\}, \quad (\text{D.7})$$

the left-right asymmetry is

$$A_{LR}^f(s) = \frac{1}{12\pi s \sigma^f(s)} \left\{ g_Z^4 \left(a_\mu^{SM} v_\mu^{SM} \left[(a_f^{SM})^2 + (v_f^{SM})^2 \right] + a_f^{SM} v_f^{SM} \left[(a_\mu^{SM})^2 + (v_\mu^{SM})^2 \right] \right) |\chi_Z|^2 + g_{Z'}^4 \left(a_f v_f \left[a_\mu^2 + v_\mu^2 \right] + a_\mu v_\mu \left[a_f^2 + v_f^2 \right] \right) |\chi_{Z'}|^2 + e^2 q_\mu q_f \left[g_Z^2 (a_f^{SM} v_\mu^{SM} + a_\mu^{SM} v_f^{SM}) \text{Re}(\chi_\gamma \chi_{Z'}^*) + g_{Z'}^2 (a_f v_\mu + a_\mu v_f) \text{Re}(\chi_\gamma \chi_{Z'}^*) \right] + g_Z^2 g_{Z'}^2 \left[(a_\mu^{SM} a_\mu + v_\mu^{SM} v_\mu) (a_f^{SM} v_f + v_f^{SM} a_f) + (a_f^{SM} a_f + v_f^{SM} v_f) (a_\mu^{SM} v_\mu + v_\mu^{SM} a_\mu) \right] \text{Re}(\chi_Z \chi_{Z'}^*) \right\}, \quad (\text{D.8})$$

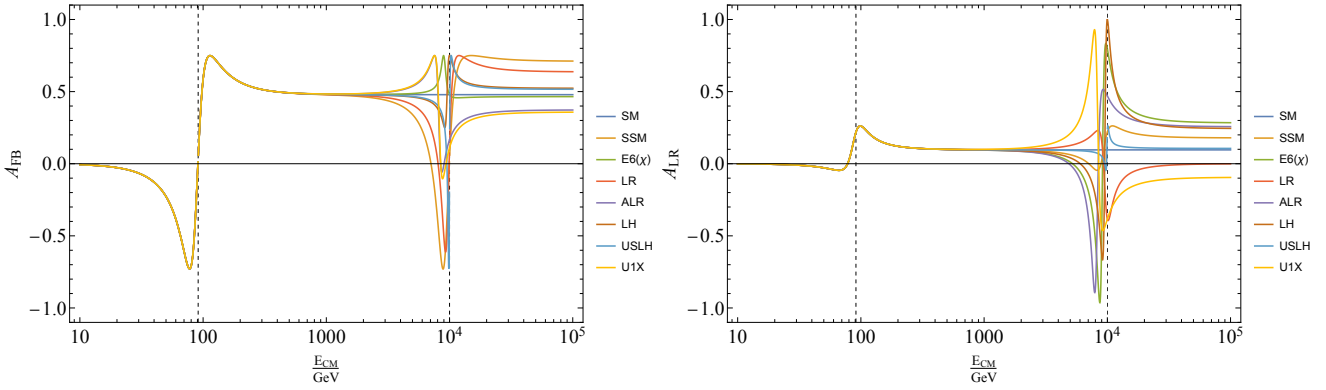


Fig. 7: We show our results for the forward-backward and left-right asymmetry that enter our χ^2 -analysis as function of the c.o.m. energy. The dashed lines lie at the mass poles at $M_Z = 91.1882 \text{ GeV}$ and $M_{Z'} = 10 \text{ TeV}$.

and for massless fermions, it holds that $A_{pol} = A_{LR}$. The total cross section in this limit is given by

$$\begin{aligned} \sigma^f(s) = \frac{1}{12\pi s} \left\{ g_Z^4 \left[(a_\mu^{SM})^2 + (v_\mu^{SM})^2 \right] \left[(a_f^{SM})^2 + (v_f^{SM})^2 \right] |\chi_Z|^2 + g_{Z'}^4 (a_\mu^2 + v_\mu^2) (a_f^2 + v_f^2) |\chi_{Z'}|^2 + e^4 q_\mu^2 q_f^2 |\chi_\gamma|^2 \right. \\ \left. + 2e^2 q_\mu q_f \left[g_Z^2 v_f^{SM} v_\mu^{SM} \text{Re}(\chi_\gamma \chi_Z^*) + g_{Z'}^2 v_f v_\mu \text{Re}(\chi_\gamma \chi_{Z'}^*) \right] \right. \\ \left. + 2g_Z^2 g_{Z'}^2 \left[a_f^{SM} a_f + v_f^{SM} v_f \right] \left[a_\mu^{SM} a_\mu + v_\mu^{SM} v_\mu \right] \text{Re}(\chi_Z \chi_{Z'}^*) \right\}. \end{aligned} \quad (\text{D.9})$$

Here, $\chi_{Z^{(\prime)}}$ are the gauge bosons propagators times a factor of s to make them dimensionless, *i.e.* the ratio of the photon propagator to considered gauge boson,

$$\chi_{Z^{(\prime)}} = \frac{s}{s + i\Gamma_{Z^{(\prime)}} M_{Z^{(\prime)}} - M_{Z^{(\prime)}}^2}, \quad (\text{D.10})$$

and $\chi_\gamma = 1$. This way of writing illustrates which interference of amplitude times conjugate amplitude is each term's origin when squaring the diagrams in Fig. 1. The distributions are shown in Fig. 7. Note that the formulae above do not hold for final state muons because one would have additional t -channel contributions there.

References

1. R. L. Workman, et al., Review of Particle Physics, PTEP 2022 (2022) 083C01. [doi:10.1093/ptep/ptac097](https://doi.org/10.1093/ptep/ptac097).
2. A. Leike, The Phenomenology of extra neutral gauge bosons, Phys. Rept. 317 (1999) 143–250. [arXiv:hep-ph/9805494](https://arxiv.org/abs/hep-ph/9805494), [doi:10.1016/S0370-1573\(98\)00133-1](https://doi.org/10.1016/S0370-1573(98)00133-1).
3. P. Langacker, The Physics of Heavy Z' Gauge Bosons, Rev. Mod. Phys. 81 (2009) 1199–1228. [arXiv:0801.1345](https://arxiv.org/abs/0801.1345), [doi:10.1103/RevModPhys.81.1199](https://doi.org/10.1103/RevModPhys.81.1199).
4. M. Aaboud, et al., Search for resonances in diphoton events at $\sqrt{s}=13 \text{ TeV}$ with the ATLAS detector, JHEP 09 (2016) 001. [arXiv:1606.03833](https://arxiv.org/abs/1606.03833), [doi:10.1007/JHEP09\(2016\)001](https://doi.org/10.1007/JHEP09(2016)001).
5. G. Aad, et al., Search for new resonances in mass distributions of jet pairs using 139 fb^{-1} of pp collisions at $\sqrt{s} = 13 \text{ TeV}$ with the ATLAS detector, JHEP 03 (2020) 145. [arXiv:1910.08447](https://arxiv.org/abs/1910.08447), [doi:10.1007/JHEP03\(2020\)145](https://doi.org/10.1007/JHEP03(2020)145).
6. G. Aad, et al., Search for high-mass dilepton resonances using 139 fb^{-1} of pp collision data collected at $\sqrt{s}=13 \text{ TeV}$ with the ATLAS detector, Phys. Lett. B 796 (2019) 68–87. [arXiv:1903.06248](https://arxiv.org/abs/1903.06248), [doi:10.1016/j.physletb.2019.07.016](https://doi.org/10.1016/j.physletb.2019.07.016).
7. A. M. Sirunyan, et al., Search for high mass dijet resonances with a new background prediction method in proton-proton collisions at $\sqrt{s} = 13 \text{ TeV}$, JHEP 05 (2020) 033. [arXiv:1911.03947](https://arxiv.org/abs/1911.03947), [doi:10.1007/JHEP05\(2020\)033](https://doi.org/10.1007/JHEP05(2020)033).
8. G. Aad, et al., Search for heavy diboson resonances in semileptonic final states in pp collisions at $\sqrt{s} = 13 \text{ TeV}$ with the ATLAS detector, Eur. Phys. J. C 80 (12) (2020) 1165. [arXiv:2004.14636](https://arxiv.org/abs/2004.14636), [doi:10.1140/epjc/s10052-020-08554-y](https://doi.org/10.1140/epjc/s10052-020-08554-y).
9. A. M. Sirunyan, et al., Search for resonant and non-resonant new phenomena in high-mass dilepton final states at $\sqrt{s} = 13 \text{ TeV}$, JHEP 07 (2021) 208. [arXiv:2103.02708](https://arxiv.org/abs/2103.02708), [doi:10.1007/JHEP07\(2021\)208](https://doi.org/10.1007/JHEP07(2021)208).

10. A. Tumasyan, et al., Search for heavy resonances decaying to WW, WZ, or WH boson pairs in the lepton plus merged jet final state in proton-proton collisions at $\sqrt{s} = 13$ TeV, *Phys. Rev. D* 105 (3) (2022) 032008. [arXiv:2109.06055](#), [doi:10.1103/PhysRevD.105.032008](#).
11. V. M. Lozano, R. M. S. Seoane, J. Zurita, Z'-explorer 2.0: Reconnoitering the dark matter landscape, *Comput. Phys. Commun.* 288 (2023) 108729. [arXiv:2109.13194](#), [doi:10.1016/j.cpc.2023.108729](#).
12. Prospects for searches for heavy Z' and W' bosons in fermionic final states with the ATLAS experiment at the HL-LHC (2018).
13. M. Cvetič, S. Godfrey, Discovery and identification of extra gauge bosons, 1995, pp. 383–415. [arXiv:hep-ph/9504216](#), [doi:10.1142/9789812830265_0007](#).
14. A. Leike, S. Riemann, Z' search in e^+e^- annihilation, *Z. Phys. C* 75 (1997) 341–348. [arXiv:hep-ph/9607306](#), [doi:10.1007/s002880050477](#).
15. S. Godfrey, P. Kalyniak, A. Tomkins, Distinguishing between models with extra gauge bosons at the ILC, in: 2005 International Linear Collider Physics and Detector Workshop and 2nd ILC Accelerator Workshop, 2005. [arXiv:hep-ph/0511335](#).
16. P. Osland, A. A. Pankov, A. V. Tsytrinov, Identification of extra neutral gauge bosons at the International Linear Collider, *Eur. Phys. J. C* 67 (2010) 191–204. [arXiv:0912.2806](#), [doi:10.1140/epjc/s10052-010-1272-z](#).
17. V. V. Andreev, G. Moortgat-Pick, P. Osland, A. A. Pankov, N. Paver, Discriminating Z' from Anomalous Trilinear Gauge Coupling Signatures in $e^+e^- \rightarrow W+W^-$ at ILC with Polarized Beams, *Eur. Phys. J. C* 72 (2012) 2147. [arXiv:1205.0866](#), [doi:10.1140/epjc/s10052-012-2147-2](#).
18. T. Han, P. Langacker, Z. Liu, L.-T. Wang, Diagnosis of a New Neutral Gauge Boson at the LHC and ILC for Snowmass 2013 (8 2013). [arXiv:1308.2738](#).
19. S. Godfrey, T. Martin, Z' Discovery Reach at Future Hadron Colliders: A Snowmass White Paper, in: Snowmass 2013: Snowmass on the Mississippi, 2013. [arXiv:1309.1688](#).
20. D. Kapukchyan, T. M. P. Tait, Sensitivity of a Future High Energy e^+e^- Collider to Z' Bosons, *J. Phys. G* 41 (2014) 075011. [arXiv:1312.3377](#), [doi:10.1088/0954-3899/41/7/075011](#).
21. A. A. Pankov, A. V. Tsytrinov, Model identification of new heavy Z' bosons at ILC with polarized beams, *J. Phys. Conf. Ser.* 938 (1) (2017) 012059. [doi:10.1088/1742-6596/938/1/012059](#).
22. A. Gulov, Y. Moroz, Optimal observables for Z' models in annihilation leptonic processes, *Phys. Rev. D* 98 (11) (2018) 115014. [arXiv:1711.02853](#), [doi:10.1103/PhysRevD.98.115014](#).
23. Z. Lu, H. Li, Z.-L. Han, Z.-G. Si, L. Zhao, Phenomenology of Heavy Neutral Gauge Boson at Muon Collider (12 2023). [arXiv:2312.17427](#).
24. S. Jindariani, et al., Promising Technologies and R&D Directions for the Future Muon Collider Detectors (3 2022). [arXiv:2203.07224](#).
25. N. Bartosik, et al., Simulated Detector Performance at the Muon Collider (3 2022). [arXiv:2203.07964](#).
26. D. Stratakis, et al., A Muon Collider Facility for Physics Discovery (3 2022). [arXiv:2203.08033](#).
27. C. Aime, et al., Muon Collider Physics Summary (3 2022). [arXiv:2203.07256](#).
28. J. de Blas, et al., The physics case of a 3 TeV muon collider stage (3 2022). [arXiv:2203.07261](#).
29. 2023 P5 Report: Exploring the Quantum Universe, <https://www.usparticlephysics.org/2023-p5-report/> (2023).
30. C. Accettura, et al., Towards a muon collider, *Eur. Phys. J. C* 83 (9) (2023) 864, [Erratum: *Eur.Phys.J.C* 84, 36 (2024)]. [arXiv:2303.08533](#), [doi:10.1140/epjc/s10052-023-11889-x](#).
31. 2020 Update of the European Strategy for Particle Physics, CERN Council, Geneva, 2020. [doi:10.17181/ESU2020](#).
32. H. Georgi, S. L. Glashow, Unity of All Elementary Particle Forces, *Phys. Rev. Lett.* 32 (1974) 438–441. [doi:10.1103/PhysRevLett.32.438](#).
33. J. C. Pati, A. Salam, Lepton Number as the Fourth Color, *Phys. Rev. D* 10 (1974) 275–289, [Erratum: *Phys.Rev.D* 11, 703–703 (1975)]. [doi:10.1103/PhysRevD.10.275](#).
34. M. Gell-Mann, P. Ramond, R. Slansky, Complex Spinors and Unified Theories, *Conf. Proc. C* 790927 (1979) 315–321. [arXiv:1306.4669](#).
35. R. Slansky, Group Theory for Unified Model Building, *Phys. Rept.* 79 (1981) 1–128. [doi:10.1016/0370-1573\(81\)90092-2](#).
36. P. Langacker, M. Plumacher, Flavor changing effects in theories with a heavy Z' boson with family nonuniversal couplings, *Phys. Rev. D* 62 (2000) 013006. [arXiv:hep-ph/0001204](#), [doi:10.1103/PhysRevD.62.013006](#).
37. S. Baek, J. H. Jeon, C. S. Kim, B0(s) - anti-B0(s) Mixing in Leptophobic Z-prime Model, *Phys. Lett. B* 641 (2006) 183–188. [arXiv:hep-ph/0607113](#), [doi:10.1016/j.physletb.2006.08.041](#).
38. E. Ma, Neutrino masses in an extended gauge model with E(6) particle content, *Phys. Lett. B* 380 (1996) 286–290. [arXiv:hep-ph/9507348](#), [doi:10.1016/0370-2693\(96\)00524-2](#).

39. E. Keith, E. Ma, Efficacious extra U(1) factor for the supersymmetric standard model, *Phys. Rev. D* 54 (1996) 3587–3593. [arXiv:hep-ph/9603353](#), [doi:10.1103/PhysRevD.54.3587](#).
40. V. Barger, P. Langacker, H.-S. Lee, Primordial nucleosynthesis constraints on Z' properties, *Phys. Rev. D* 67 (2003) 075009. [arXiv:hep-ph/0302066](#), [doi:10.1103/PhysRevD.67.075009](#).
41. J.-h. Kang, P. Langacker, T.-j. Li, Neutrino masses in supersymmetric SU(3)(C) x SU(2)(L) x U(1)(Y) x U(1)-prime models, *Phys. Rev. D* 71 (2005) 015012. [arXiv:hep-ph/0411404](#), [doi:10.1103/PhysRevD.71.015012](#).
42. S. F. King, S. Moretti, R. Nevzorov, Theory and phenomenology of an exceptional supersymmetric standard model, *Phys. Rev. D* 73 (2006) 035009. [arXiv:hep-ph/0510419](#), [doi:10.1103/PhysRevD.73.035009](#).
43. R. N. Mohapatra, J. C. Pati, A Natural Left-Right Symmetry, *Phys. Rev. D* 11 (1975) 2558. [doi:10.1103/PhysRevD.11.2558](#).
44. B. de Carlos, J. R. Espinosa, Cold dark matter candidate in a class of supersymmetric models with an extra U(1), *Phys. Lett. B* 407 (1997) 12–21. [arXiv:hep-ph/9705315](#), [doi:10.1016/S0370-2693\(97\)00747-8](#).
45. S. Nakamura, D. Suematsu, Supersymmetric extra U(1) models with a singlino dominated LSP, *Phys. Rev. D* 75 (2007) 055004. [arXiv:hep-ph/0609061](#), [doi:10.1103/PhysRevD.75.055004](#).
46. V. Barger, P. Langacker, I. Lewis, M. McCaskey, G. Shaughnessy, B. Yencho, Recoil Detection of the Lightest Neutralino in MSSM Singlet Extensions, *Phys. Rev. D* 75 (2007) 115002. [arXiv:hep-ph/0702036](#), [doi:10.1103/PhysRevD.75.115002](#).
47. H.-S. Lee, K. T. Matchev, S. Nasri, Revival of the thermal sneutrino dark matter, *Phys. Rev. D* 76 (2007) 041302. [arXiv:hep-ph/0702223](#), [doi:10.1103/PhysRevD.76.041302](#).
48. G. Belanger, A. Pukhov, G. Servant, Dirac Neutrino Dark Matter, *JCAP* 01 (2008) 009. [arXiv:0706.0526](#), [doi:10.1088/1475-7516/2008/01/009](#).
49. J. L. Hewett, T. G. Rizzo, Low-Energy Phenomenology of Superstring Inspired E(6) Models, *Phys. Rept.* 183 (1989) 193. [doi:10.1016/0370-1573\(89\)90071-9](#).
50. V. D. Barger, W.-Y. Keung, E. Ma, Sequential W and Z Bosons, *Phys. Lett. B* 94 (1980) 377–380. [doi:10.1016/0370-2693\(80\)90900-4](#).
51. R. W. Robinett, J. L. Rosner, Prospects for a Second Neutral Vector Boson at Low Mass in SO(10), *Phys. Rev. D* 25 (1982) 3036, [Erratum: *Phys. Rev. D* 27, 679 (1983)]. [doi:10.1103/PhysRevD.27.679](#).
52. G. Altarelli, B. Mele, M. Ruiz-Altaba, Searching for New Heavy Vector Bosons in $p\bar{p}$ Colliders, *Z. Phys.* C 45 (1989) 109, [Erratum: *Z. Phys. C* 47, 676 (1990)]. [doi:10.1007/BF01556677](#).
53. Y. Achiman, B. Stech, Quark-lepton symmetry and mass scales in an e_6 unified gauge model, *Physics Letters B* 77 (4-5) (1978) 389–393.
54. D. London, J. L. Rosner, Extra Gauge Bosons in E(6), *Phys. Rev. D* 34 (1986) 1530. [doi:10.1103/PhysRevD.34.1530](#).
55. R. N. Mohapatra, G. Senjanovic, Neutrino Mass and Spontaneous Parity Nonconservation, *Phys. Rev. Lett.* 44 (1980) 912. [doi:10.1103/PhysRevLett.44.912](#).
56. R. N. Mohapatra, G. Senjanovic, Neutrino Masses and Mixings in Gauge Models with Spontaneous Parity Violation, *Phys. Rev. D* 23 (1981) 165. [doi:10.1103/PhysRevD.23.165](#).
57. E. Ma, Particle dichotomy and left-right decomposition of e_6 superstring models, *Phys. Rev. D* 36 (1987) 274–276. [doi:10.1103/PhysRevD.36.274](#).
URL <https://link.aps.org/doi/10.1103/PhysRevD.36.274>
58. M. Ashry, S. Khalil, Phenomenological aspects of a TeV-scale alternative left-right model, *Physical Review D* 91 (1) (jan 2015). [doi:10.1103/physrevd.91.015009](#).
URL <https://doi.org/10.1103%2Fphysrevd.91.015009>
59. N. Arkani-Hamed, A. G. Cohen, E. Katz, A. E. Nelson, The Littlest Higgs, *JHEP* 07 (2002) 034. [arXiv:hep-ph/0206021](#), [doi:10.1088/1126-6708/2002/07/034](#).
60. T. Han, H. E. Logan, B. McElrath, L.-T. Wang, Phenomenology of the little Higgs model, *Phys. Rev. D* 67 (2003) 095004. [arXiv:hep-ph/0301040](#), [doi:10.1103/PhysRevD.67.095004](#).
61. W. Kilian, J. Reuter, The Low-energy structure of little Higgs models, *Phys. Rev. D* 70 (2004) 015004. [arXiv:hep-ph/0311095](#), [doi:10.1103/PhysRevD.70.015004](#).
62. M. Schmaltz, The Simplest little Higgs, *JHEP* 08 (2004) 056. [arXiv:hep-ph/0407143](#), [doi:10.1088/1126-6708/2004/08/056](#).
63. W. Kilian, D. Rainwater, J. Reuter, Pseudo-axions in little Higgs models, *Phys. Rev. D* 71 (2005) 015008. [arXiv:hep-ph/0411213](#), [doi:10.1103/PhysRevD.71.015008](#).
64. W. Kilian, D. Rainwater, J. Reuter, Distinguishing little-Higgs product and simple group models at the LHC and ILC, *Phys. Rev. D* 74 (2006) 095003, [Erratum: *Phys. Rev. D* 74, 099905 (2006)]. [arXiv:hep-ph/0609119](#), [doi:10.1103/PhysRevD.74.095003](#).
65. S. Oda, N. Okada, D.-s. Takahashi, Classically conformal U(1)' extended standard model and Higgs vacuum stability, *Phys. Rev. D* 92 (1) (2015) 015026. [arXiv:](#)

- 1504.06291, doi:10.1103/PhysRevD.92.015026.
66. S. Iso, N. Okada, Y. Orikasa, Classically conformal b–l extended standard model, *Physics Letters B* 676 (1-3) (2009) 81–87.
 67. H. Fritzsch, P. Minkowski, Unified Interactions of Leptons and Hadrons, *Annals Phys.* 93 (1975) 193–266. doi:10.1016/0003-4916(75)90211-0.
 68. A. de Rújula, H. Georgi, S. L. Glashow, Trinification of All Elementary Particle Forces, in: *Fifth Workshop on Grand Unification*, 1984.
 69. W. Kilian, J. Reuter, Unification without doublet-triplet splitting, *Phys. Lett. B* 642 (2006) 81–84. arXiv:hep-ph/0606277, doi:10.1016/j.physletb.2006.09.033.
 70. F. Braam, A. Knochel, J. Reuter, An Exceptional SSM from E6 Orbifold GUTs with intermediate LR symmetry, *JHEP* 06 (2010) 013. arXiv:1001.4074, doi:10.1007/JHEP06(2010)013.
 71. F. Braam, J. Reuter, A Simplified Scheme for GUT-inspired Theories with Multiple Abelian Factors, *Eur. Phys. J. C* 72 (2012) 1885. arXiv:1107.2806, doi:10.1140/epjc/s10052-012-1885-5.
 72. T. G. Rizzo, Gauge Kinetic Mixing in the E_6 SSM, *Phys. Rev. D* 85 (2012) 055010. arXiv:1201.2898, doi:10.1103/PhysRevD.85.055010.
 73. L. Randall, R. Sundrum, A Large mass hierarchy from a small extra dimension, *Phys. Rev. Lett.* 83 (1999) 3370–3373. arXiv:hep-ph/9905221, doi:10.1103/PhysRevLett.83.3370.
 74. T. Appelquist, H.-C. Cheng, B. A. Dobrescu, Bounds on universal extra dimensions, *Phys. Rev. D* 64 (2001) 035002. arXiv:hep-ph/0012100, doi:10.1103/PhysRevD.64.035002.
 75. T. Han, J. D. Lykken, R.-J. Zhang, On Kaluza-Klein states from large extra dimensions, *Phys. Rev. D* 59 (1999) 105006. arXiv:hep-ph/9811350, doi:10.1103/PhysRevD.59.105006.
 76. A. Heister, et al., Measurement of the tau polarization at LEP, *Eur. Phys. J. C* 20 (2001) 401–430. arXiv:hep-ex/0104038, doi:10.1007/s100520100689.
 77. P. Abreu, et al., A Precise measurement of the tau polarization at LEP-1, *Eur. Phys. J. C* 14 (2000) 585–611. doi:10.1007/s100520000363.
 78. K. Mekala, D. Jeans, J. Tian, J. Reuter, A. F. Żarnecki, Precise measurement of light-quark electroweak couplings at future colliders, presented at the Epiphany’24 conference, <https://indico.cern.ch/event/1288528/contributions/5718576/> (2024).
 79. I. Zurbano Fernandez, et al., High-Luminosity Large Hadron Collider (HL-LHC): Technical design report 10/2020 (12 2020). doi:10.23731/CYRM-2020-0010.
 80. The International Linear Collider Technical Design Report - Volume 2: Physics (6 2013). arXiv:1306.6352.
 81. H. Abramowicz, et al., The International Linear Collider Technical Design Report - Volume 4: Detectors (6 2013). arXiv:1306.6329.
 82. A. Abada, et al., FCC-ee: The Lepton Collider: Future Circular Collider Conceptual Design Report Volume 2, *Eur. Phys. J. ST* 228 (2) (2019) 261–623. doi:10.1140/epjst/e2019-900045-4.
 83. W. Abdallah, et al., CEPC Technical Design Report – Accelerator (v2) (12 2023). arXiv:2312.14363.
 84. A Multi-TeV Linear Collider Based on CLIC Technology: CLIC Conceptual Design Report (10 2012). doi:10.5170/CERN-2012-007.
 85. Physics and Detectors at CLIC: CLIC Conceptual Design Report (2 2012). arXiv:1202.5940, doi:10.5170/CERN-2012-003.
 86. A. Abada, et al., FCC-hh: The Hadron Collider: Future Circular Collider Conceptual Design Report Volume 3, *Eur. Phys. J. ST* 228 (4) (2019) 755–1107. doi:10.1140/epjst/e2019-900087-0.
 87. A. Abada, et al., FCC Physics Opportunities: Future Circular Collider Conceptual Design Report Volume 1, *Eur. Phys. J. C* 79 (6) (2019) 474. doi:10.1140/epjc/s10052-019-6904-3.
 88. J. Tang, et al., Concept for a Future Super Proton-Proton Collider (7 2015). arXiv:1507.03224.
 89. M. Bogomilov, et al., Demonstration of cooling by the Muon Ionization Cooling Experiment, *Nature* 578 (7793) (2020) 53–59. arXiv:1907.08562, doi:10.1038/s41586-020-1958-9.
 90. J. Chen, T. Han, B. Tweedie, Electroweak Splitting Functions and High Energy Showering, *JHEP* 11 (2017) 093. arXiv:1611.00788, doi:10.1007/JHEP11(2017)093.
 91. T. Han, Y. Ma, K. Xie, High energy leptonic collisions and electroweak parton distribution functions, *Phys. Rev. D* 103 (3) (2021) L031301. arXiv:2007.14300, doi:10.1103/PhysRevD.103.L031301.
 92. F. Garosi, D. Marzocca, S. Trifinopoulos, LePDF: Standard Model PDFs for high-energy lepton colliders, *JHEP* 09 (2023) 107. arXiv:2303.16964, doi:10.1007/JHEP09(2023)107.
 93. W. Kilian, T. Ohl, J. Reuter, Whizard—simulating multi-particle processes at lhc and ilc, *The European Physical Journal C* 71 (9) (Sep. 2011). doi:10.1140/epjc/s10052-011-1742-y. URL <http://dx.doi.org/10.1140/epjc/s10052-011-1742-y>
 94. M. Moretti, T. Ohl, J. Reuter, O’mega: An optimizing matrix element generator (2001). arXiv:hep-ph/0102195.

-
95. N. D. Christensen, C. Duhr, B. Fuks, J. Reuter, C. Speckner, Introducing an interface between WHIZARD and FeynRules, *Eur. Phys. J. C* 72 (2012) 1990. [arXiv:1010.3251](https://arxiv.org/abs/1010.3251), [doi:10.1140/epjc/s10052-012-1990-5](https://doi.org/10.1140/epjc/s10052-012-1990-5).
96. C. Degrande, C. Duhr, B. Fuks, D. Grellscheid, O. Matelaer, T. Reiter, UFO - The Universal FeynRules Output, *Comput. Phys. Commun.* 183 (2012) 1201–1214. [arXiv:1108.2040](https://arxiv.org/abs/1108.2040), [doi:10.1016/j.cpc.2012.01.022](https://doi.org/10.1016/j.cpc.2012.01.022).
97. L. Darmé, et al., UFO 2.0: the ‘Universal Feynman Output’ format, *Eur. Phys. J. C* 83 (7) (2023) 631. [arXiv:2304.09883](https://arxiv.org/abs/2304.09883), [doi:10.1140/epjc/s10052-023-11780-9](https://doi.org/10.1140/epjc/s10052-023-11780-9).
98. P. M. Bredt, W. Kilian, J. Reuter, P. Stenemeier, NLO electroweak corrections to multi-boson processes at a muon collider, *JHEP* 12 (2022) 138. [arXiv:2208.09438](https://arxiv.org/abs/2208.09438), [doi:10.1007/JHEP12\(2022\)138](https://doi.org/10.1007/JHEP12(2022)138).